Chapter 3

Flame Retardant Polymer Nanocomposites and Interfaces

Yuan Xue, Yichen Guo* and Miriam H. Rafailovich

Additional information is available at the end of the chapter

http://dx.doi.org/10.5772/intechopen.79548

Abstract

The flame retardant efficiency of polymer nanocomposites is highly dependent on the dispersion of the nano-fillers within the polymer matrix. In order to control the filler dispersion, it is very essential to explore the interfacial compatibility between fillers and matrices, which provides a guide for the flame retardant nanocomposites compounding. In this short review, we mainly focus on the thermoplastic polymers and their interactions with the surfaces of the flame retardant fillers. Other physical properties of those nanocomposites such as mechanical properties, gas permeability, rheological performance and thermal conductivity are also briefly reviewed along with the flame retardancy, since they are all dispersion related.

Keywords: polymer nanocomposites, filler dispersion, interfacial compatibility, flame retardancy, mechanical properties

1. Introduction

In past decades, polymeric materials have been extensively used in construction, transportation, and electronic devices due to the high performance and cost-effectiveness [1]. However, most of the polymeric materials were intrinsically combustible, which caused the fire hazard. The necessity to improve the flame retardancy of polymeric materials was urgent, so that people started to incorporate flame retardants into polymers to produce flame retardant polymer composites. The commercial used flame retardants mainly included endothermic additives, halogenated additives, phosphorus additives, expandable graphite and melamine derivatives. However, using a single component flame retardant to make the polymer reach the desired flame retardant performance required high loading of additives, which can cause

the deterioration of the mechanical properties of the polymer matrix. In order to enhance the flame retardant efficiency of additives, synergistic flame retardant systems were developed [2–6]. These systems contained two or more additives. Some additives were not flame retardant themselves, but can effectively synergize the performance with other flame retardants, thereby minimizing the total loading of the additives within the polymer matrices. The most common combinations, such as antimony oxides [7]/halogens [8], metal hydroxides [9–11]/zinc borate [12], and intumescent phosphates [13, 14] have already been widely used in various polymers and successfully commercialized. Recently, people started to use nano-scale additives to make polymer nanocomposites and expect further enhancement of the flame retardant performance. The practice of mixing nanoparticles with polymers to make polymer nanocomposites can be traced back to nineteenth century [15, 16]. Those composite materials inherited the properties of the nanoparticles and showed significant enhancement in performance compared to their polymeric matrices. However, the mechanisms for the reinforcement of the polymeric matrices by nanoparticles were not adequately understood until 1990s. This rise of polymer nanocomposites research benefitted from the growing availability of nanoparticles and the emergence of instrumentation to probe the nano-scale structure of materials [17]. Furthermore, powerful computers allowed for the development of theoretical models which together with experiments were used to develop the guiding principles for engineering new nanocomposites with desirable properties. These models highlighted the critical role of surface and interfacial energies between the fillers and the polymer matrix and as well as the role particle morphology. Consequently, research of flame retardant polymer nanocomposites has been widely reported from both academic and industrial laboratories [18, 19].

In this review, we will mainly focus on the thermoplastic polymer based nanocomposites. Comparing to the thermoset polymer nanocomposites, thermoplastic polymer nanocomposites are easy to process and formulate in manufacturing, which makes them a very diverse and manageable composite system. This review describes the mechanisms of interaction between singular or binary thermoplastic polymer matrices with the commonly used nanoparticles: montmorillonite clay, graphene, nature nanotubes and fibers. The effect of nanoparticles influence on flame retardant efficiency was discussed, as well as the change in physical properties, such as impact resistance, ductility, gas permeability and rheology performance.

2. Singular polymer matrix

2.1. Montmorillonite clays

Montmorillonite is one of the most commonly used fillers in materials application. It could be dispersed in a polymer matrix to form polymer-clay nanocomposite. Okamoto et al. have shown that the organically modified montmorillonite clay could improve the thermal mechanical and gas barrier effect of poly (lactic acid) (PLA) [20]. By using wide-angle X-ray diffraction and transmission electron microscopy, they found that with the differences in clay modification, four different types of clay-polymer morphology were formed: intercalated,

http://dx.doi.org/10.5772/intechopen.79548

intercalated-and-flocculated, exfoliated and coexistence of intercalated and exfoliated. The intercalated structure achieved great mechanical property improvement, and the near exfoliated composite has the highest gas barrier effect. However, the mechanism of the surface interaction was not well developed. Also, to improve the degree of exfoliation of clay platelets, cation exchange with quaternary ammonium chloride salts was commonly used for clay modification. The development of this method was held back due to the toxicity of these salts [21].

Recently, Guo et al. developed a much efficient way to determine the affinity between large aspect ratio nanoparticles and the polymer matrix by simply measuring the Young's contact angle [22]. The relative affinity between PLA and Closite Na^+ clay/Closite 30B (C-30B) clay were studied. They also used resorcinol di(phenyl phosphate) (RDP) adsorption to modify the Closite Na^+ clay (C-Na^+), which has been proven to perform better than using organoclays alone in conventional polymer systems [23]. The chemical formula of RDP is shown in **Figure 1**. With the nonpolar moieties of phenol groups and polar moieties of phosphoric acids groups, RDP could be used as a surfactant [24]. It has also been proven to react with polymers at high temperatures to form chars, which renders its ability to work as a flame retardant additive [25, 26]. In this research, a monolayer of these clay particles were formed on Si wafer using Langmuir–Blodgett (LB) technique. A 5 mg PLA pellet was melted on top of each clay monolayer and the Young's contact angles at the polymer/clay surface/air interface were measured. The procedure is illustrated in **Figure 2**. Then with the combination of the interfacial energy equation and the equation for work of adhesion (W_a), the relationship between W_a and Young's contact angle (A) was developed as below:

$$W_a = \gamma_l(1 + \cos A)$$

whereγ_l is the surface tension of liquid phase, which is PLA in this case. By substituting the measured contact angle and calculate the individual W_a between PLA and each clay (listed in **Figure 2**), they found that comparing to the original MMT clay C-Na^+, the synthesized C-30B clay and the C-RDP clay were more compatible to the PLA matrix. Further small angle scattering (SAXS) and TEM results, shown in **Figure 3**, confirmed that there is no change on the interlayer spacing of C-Na^+ clay and they formed tactoids inside the polymer matrix.

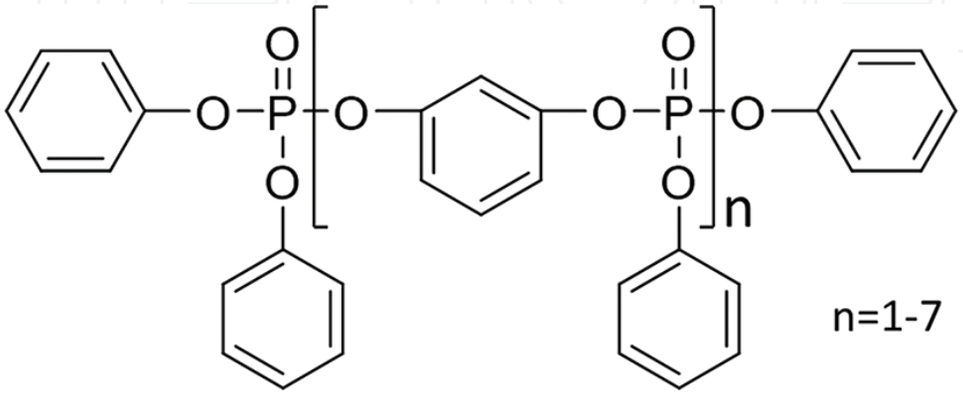

Figure 1. The chemical formula of RDP.

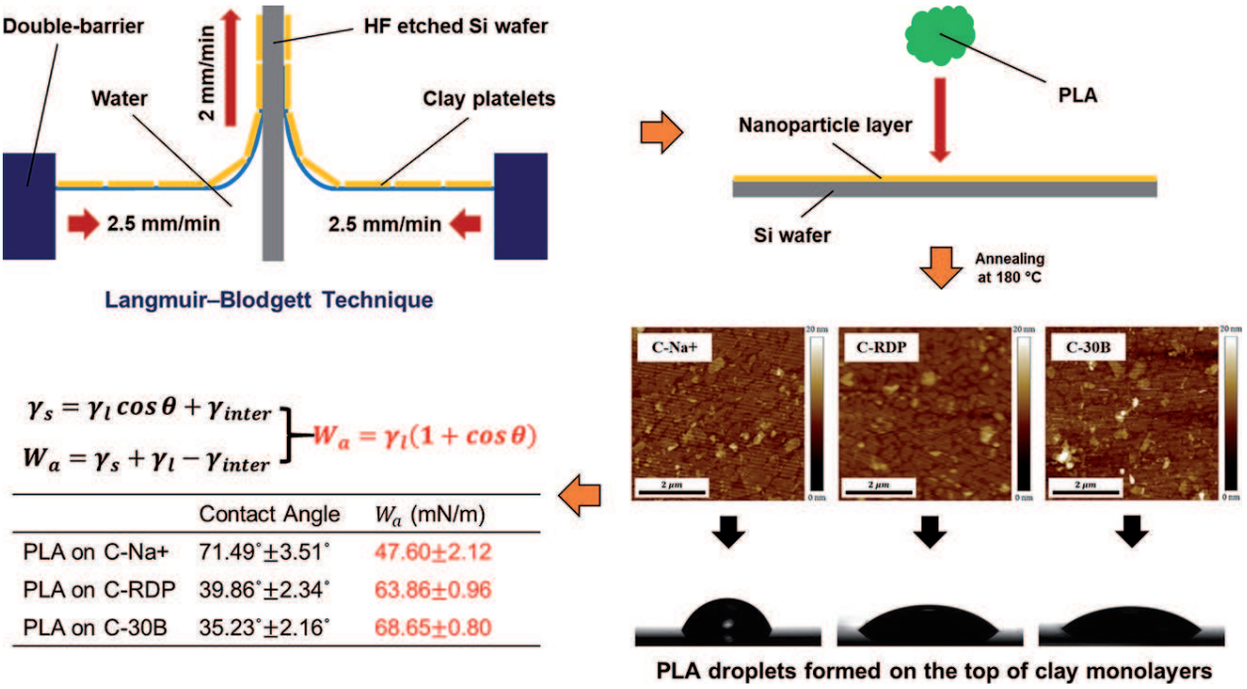

$$\gamma_s = \gamma_l \cos\theta + \gamma_{inter}$$
$$W_a = \gamma_s + \gamma_l - \gamma_{inter}$$
$$\Rightarrow W_a = \gamma_l(1 + \cos\theta)$$

	Contact Angle	W_a (mN/m)
PLA on C-Na+	71.49°±3.51°	47.60±2.12
PLA on C-RDP	39.86°±2.34°	63.86±0.96
PLA on C-30B	35.23°±2.16°	68.65±0.80

Figure 2. An illustration of creating monolayer of nanoparticle by LB technique, and a list of measure contact angle of PLA on each type of clay with calculated work of adhesion. Adapted from Ref. [22]. Copyright (2018) with permission from Elsevier.

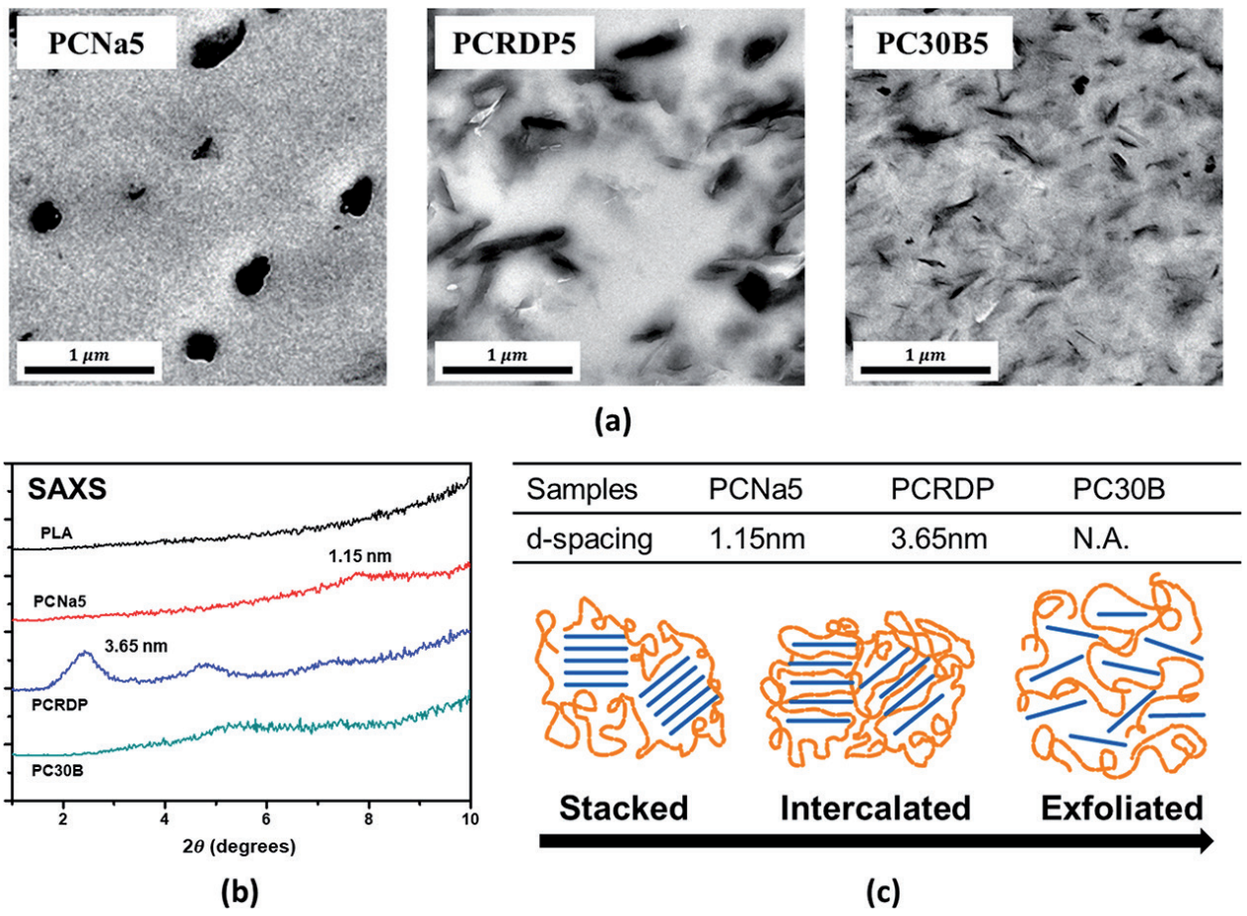

Figure 3. TEM imaging and X-ray pattern of PLA/clay composites: (a) TEM images of PLA/C-Na^+ blend (PCNa5), PLA/C-RDP blend (PCRDP5) and PLA/C-30B blend (PC30B5); (b) small angle X-ray scattering patterns of pure PLA and composites with clays. Adapted from Ref. [22]. Copyright (2018) with permission from Elsevier.

The interlayer spacing for C-RDP increased from 2.04 to 3.65 nm, which indicates the polymer chains intercalated with the clay platelets. In the case for C-30B, the SAXS pattern only showed a weak secondary (002) peak which proved that the C-30B platelets were exfoliated. These results are in good agreement with the previous W_a measurement, which concludes that the work of adhesion between the clay platelets and polymer needs to increase to achieve particle exfoliation inside polymer matrix.

Since C-30B are mostly exfoliated in the PLA matrix, Guo et al. continued to study its possible effect on improving the performance of flame retardant agent [4]. As a biodegradable polymeric material with good mechanical and processing properties, PLA has been extensively studied over recent years and has been used as a substitution for conventional polymers [27, 28]. In order to expand its usage into electron devices and automobile industry, the high flammability of PLA must be resolved. Melamine polyphosphate (MPP) was used in this study, which is a halogen-free flame retardant agent [29]. When used alone, 28 wt.% of MPP is needed to achieve the V0 grade in UL-94 vertical burning test. TEM images in **Figure 4(a)** showed that the MPP formed droplet shaped domains with a diameter around 500 nm. According to Araki et al., when large aspect ratio particles were used to compatible a binary system, the domain size is controlled by balancing between the reduction of system enthalpy and the increase of bending energy due to particle curvature [30], and the minimum domain size should be similar to the radius of particle platelets. When 1 wt.% of C-30B is added to the system, the MPP were better dispersed and the domain size were reduced to around 150 nm, which is similar to the radius of C-30B platelets. And only 17 wt.% of MPP is needed to obtain the V0 grade, as

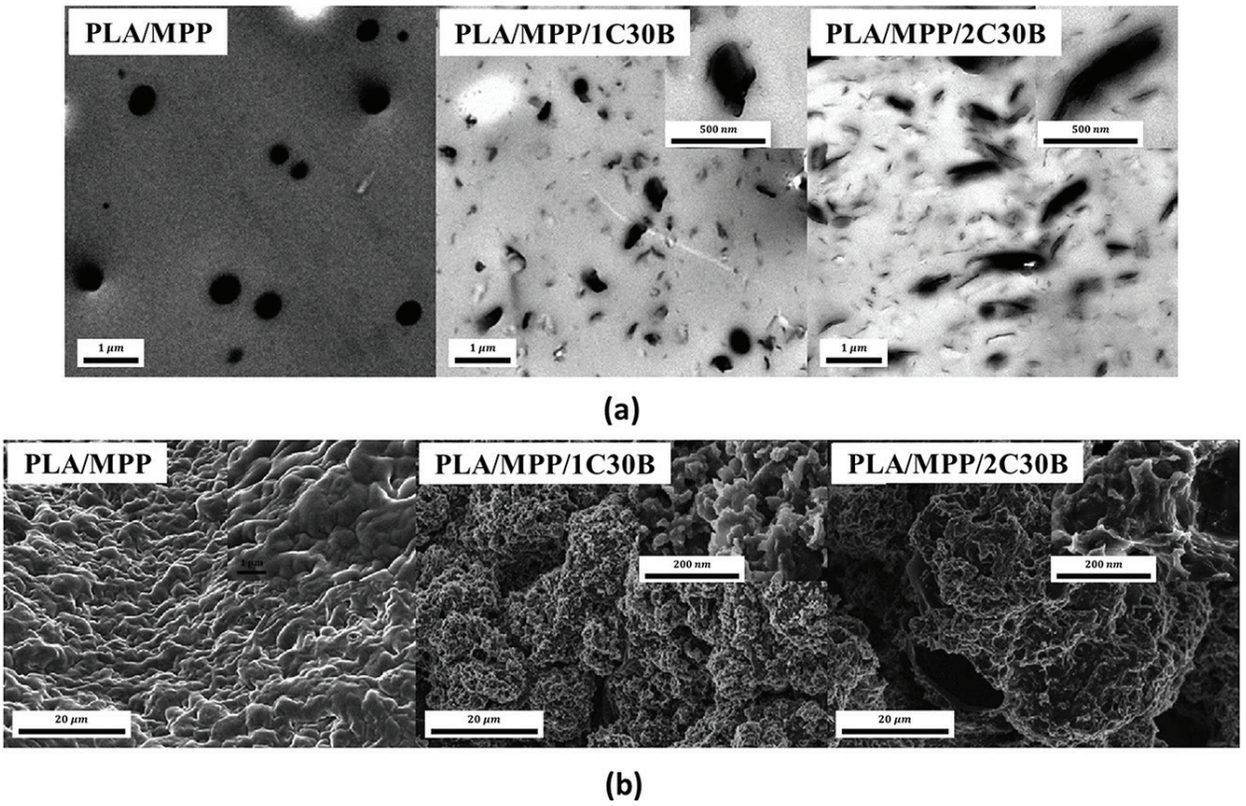

Figure 4. TEM and SEM images of PLA/MPP/C-30B blends: (a) TEM images taken on cross-sections of PLA composites; (b) SEM images on the char residue after cone calorimetry test. Adapted from Ref. [4]. Copyright (2018) with permission from Elsevier.

Sample	Avg. heat release rate (kW/m^2)	Peak heat release rate (kW/m^2)	Total heat release (MJ/m^2)
100PLA	6–1120	1.1–29.0	80–920
PLA/MPP	117.5	12.6	359
PLA/MPP/1C-30B	239.7	17.3	441
PLA/MPP/2C-30B	133.3	13.4	348

Table 1. Cone calorimetry results of PLA/MPP/C-30B blends. Adapted from Ref. [4]. Copyright (2018) with permission from Elsevier.

oppose to the previous 28%. However, further increase C-30B concentration to 2% resulted in enlarged and elongated MPP domain, which is to reduce the energy penalty brought by bending clay particles. And C-30B starts to form aggregates on the elongated MPP domain surface, which blocked the contact of polyphosphate to the PLA molecules. In the cone calorimetry test (listed in **Table 1**), the better dispersed MPP/1%C-30B system has lower average heat release rate (aHRR), peak heat release rate (pHRR) and total heat release (THR) than MPP with 2% C-30B. Examination of char residue also agree with this result. Intumescent char layers were found for both samples with only MPP and MPP/1% C-30B. As shown in **Figure 4(b)**, the char layer of sample with only MPP is continuous and has a winkled structure due to the gas inflating during heating and releasing after cooling. Similar winkled structure was found on the char layer of sample containing MPP/1% C-30B, where the winkle was formed by dense polymer/clay aggregates. In contrast, the char layer of sample with MPP/2% C-30B was loose and powdery, which is composed of large polymer/clay agglomerates and has numerous micro-cracks. This result confirmed their theory that when clay platelets were exfoliated and act as a dispersant, the MPP is better dispersed which could increase the flame retardant efficiency. The exfoliated clay platelets also provide large surface area to interact with both polymer chain and MPP, improving the formation of the intumescent char. Yet the window of improvement is limited because further increasing clay content would result in clay aggregating on the polymer/FR interface and harming the FR performance.

2.2. Graphene

Having a similar platelet structure to clay, graphene is also a large aspect ratio nanoparticle and has gained great attention in many research areas due to its superior thermal conductivity, heat sink effect and great mechanical performance [31–33]. Given the large surface area and heat adsorption of graphene, Xue et al. developed a three component flame retardant ethylene vinyl acetate (EVA) composite as a replacement of polyvinyl chloride (PVC) for cable sheathing [6]. The three component FR system consists of aluminum hydroxide (ATH), molybdenum disulfide (MoS_2) and graphene nanoplatelets (GNPs). When ATH was used alone, it could absorb heat and release water vapor during combustion, which could dilute the oxygen surround the sample surface. However, due to the poor compatibility between ATH and EVA, ATH would form large aggregates in the polymer matrix, which decreased the interfacial area for ATH to react and therefore decreasing its efficiency, as shown in the TEM

http://dx.doi.org/10.5772/intechopen.79548

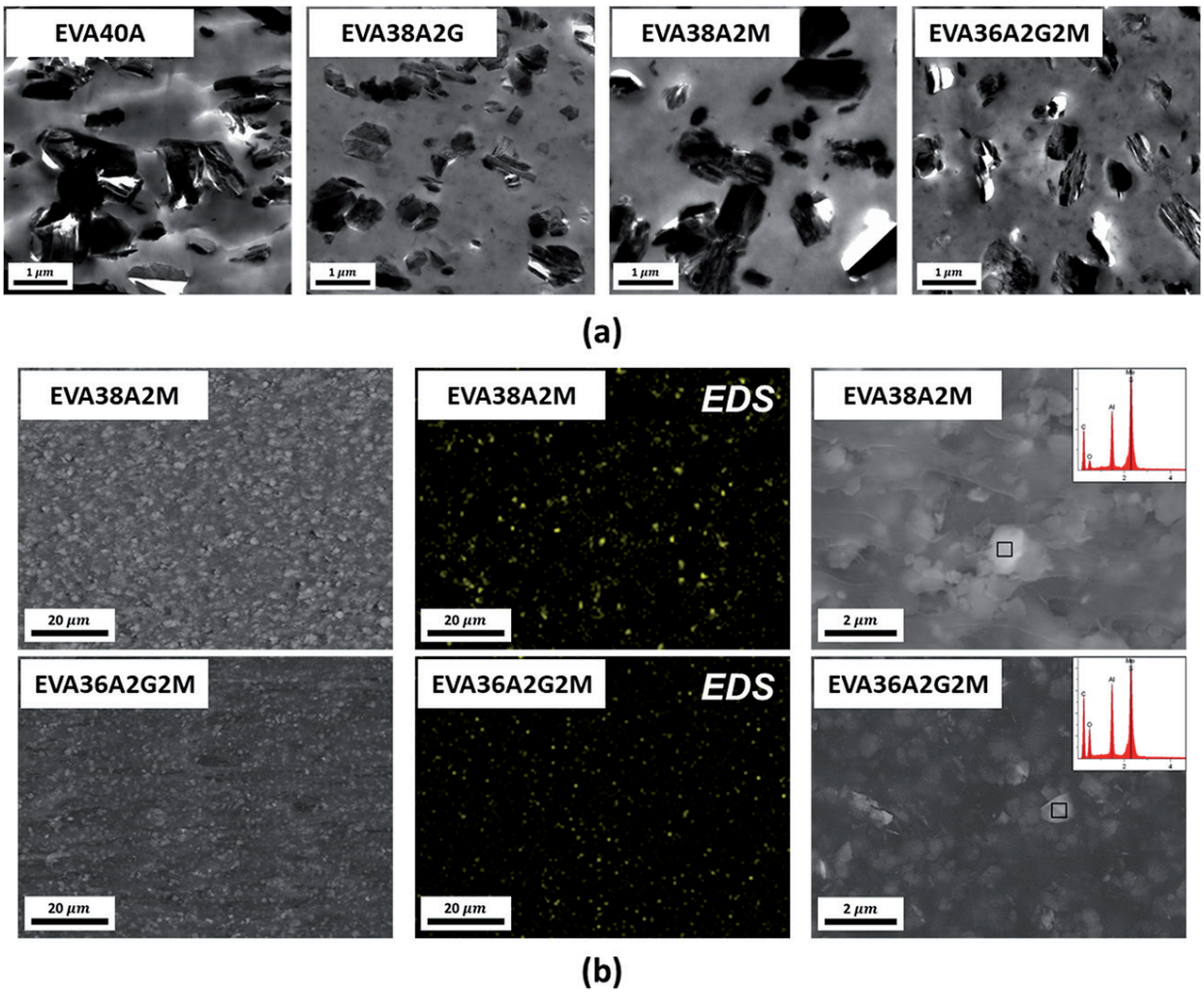

Figure 5. (a) TEM images taken on cross-sections of EVA based composites; (b) SEM and EDS mapping of EVA based composites. Annotations of abbreviations used: A—ATH, M—MoS_2, G—GNPs and numbers stands for weight ratio. Adapted from Ref. [6]. Copyright (2018) with permission from Elsevier.

images in **Figure 5(a)**. As a result, 50–60 wt.% of ATH is needed to achieve the V0 grade in UL-94 test, which will greatly decrease the ductility of EVA. When substituting 2 wt.% of ATH to MoS_2, the PHRR was reduced but a sharp peak is still observed on the heat release curve, as seen in **Figure 6**. This is because MoS_2 have formed tactoids in EVA matrix, which decreased their surface area and reducing its ability to form protective char layer. On the other hand, when further substituting 2 wt.% of ATH to GNPs, a better dispersion was observed for both ATH and MoS_2 and the heat release curve was flattened. TEM images showed that the domain size of ATH is greatly reduced and EDS mapping (**Figure 5(b)**) showed that MoS_2 was partially exfoliated. This is contributed to the large surface area of graphene platelets, which could react at the polymer/filler interface and reducing the interfacial tension. Thus, as shown in **Scheme 1**, when the EVA composite with the three-component FR system was subject to high heat flux or flame, the ATH has a higher efficiency on absorbing heat and releasing water vapor due to the improved dispersion. The exfoliated MoS_2 and GNPs will form protective char layer on the sample surface, which could reduce the peak heat release rate and flatten

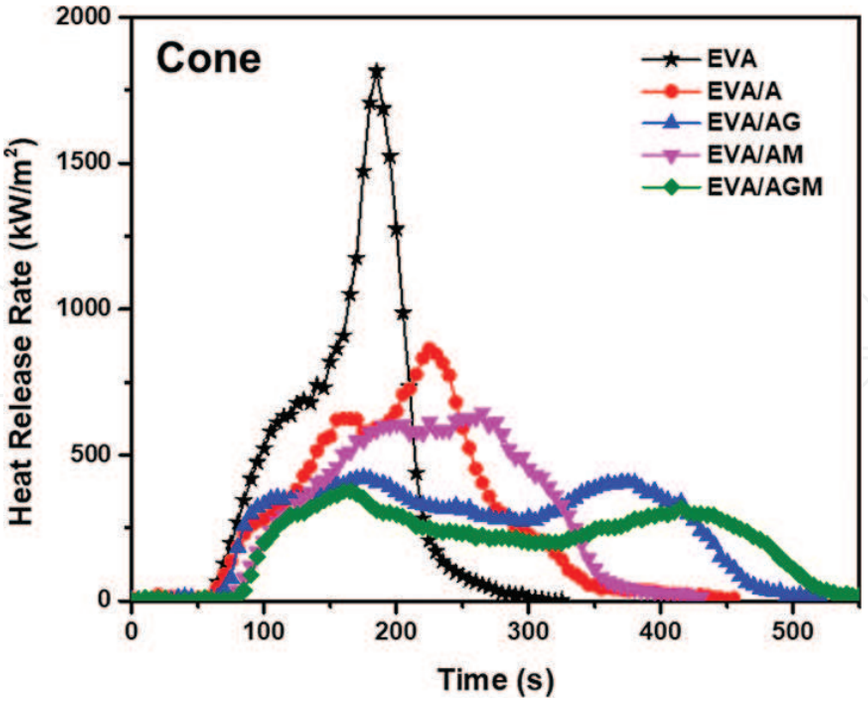

Figure 6. Cone calorimetry results of EVA composites. Reproduced from Ref. [6]. Copyright (2018) with permission from Elsevier.

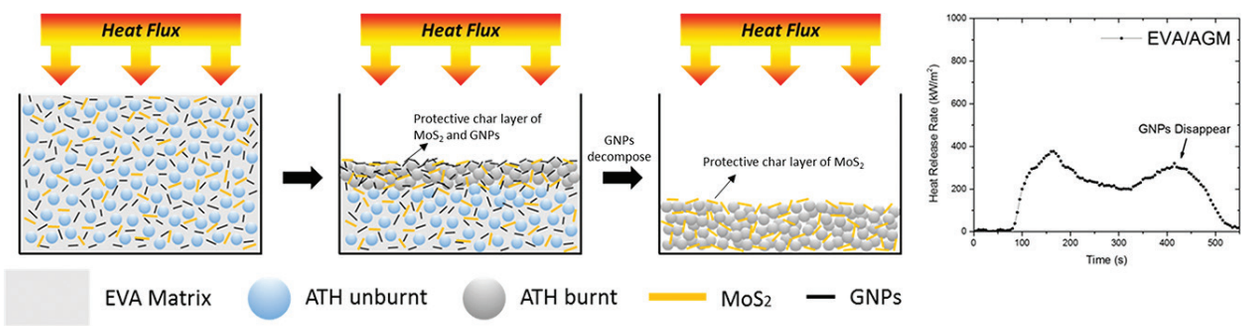

Scheme 1. The decomposition process of EVA/ATH/MoS_2/GNPs composite. Adapted from Ref. [6]. Copyright (2018) with permission from Elsevier.

the heat release curve. The GNPs will start to decompose at around 635°C, but the MoS_2 layer will continue to control the heat release. As a result, this EVA-ATH-MoS_2-GNPs composite has a PHRR of 377 kW/m^2, which is a huge reduction comparing to that of pure EVA, which is 1815 kW/m^2.

2.3. Natural nanotubes and fibers

Nanotubes such as carbon nanotube, Halloysite nanotube (HNTs), and cellulose fibers have gained increasing attentions in recent years to replace filler that have high environmental persistence [34–36]. They could also render the polymer composite to have increased mechanical properties [37]. When applied in the flame retardant composites, surface modification is commonly used to increase the flame retardancy. As previous mentioned, resorcinol bis (diphenyl

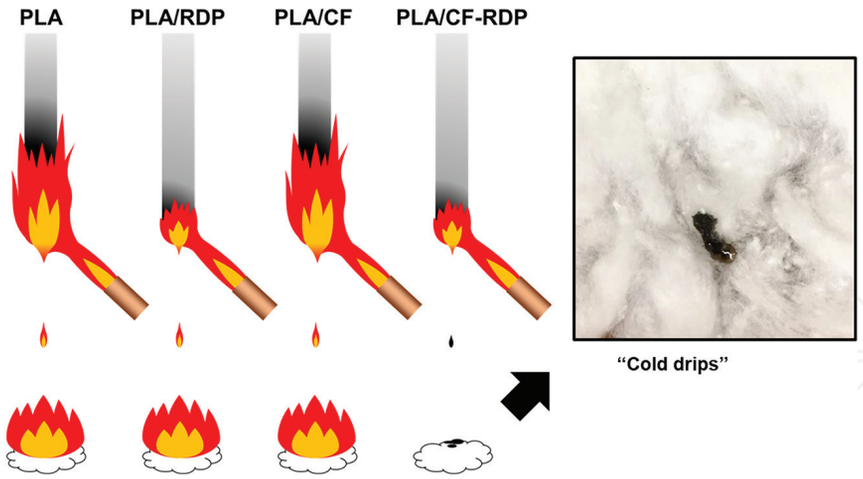

Scheme 2. An illustration of the UL-94 test process of PLA based composites. CF stands for cellulose fiber. Adapted from Ref. [5]. Copyright (2018) with permission from Elsevier.

phosphate) (RDP) is a liquid form flame retardant, which could be adsorbed on to fillers with hydroxyl groups. In the previously mentioned study [22], Guo et al. have also compared the change of work of adhesion between PLA and HNTs, with and without the RDP coating. They found that RDP coated HNTs had a higher work of adhesion to PLA than pure HNTs, which indicated that PLA wetted the RDP coating, and RDP could successfully improve the dispersion of HNTs. Thus, they used the same methodology to develop a new flame retardant PLA composite using RDP coated cellulose [5]. When subjected to flame, pure PLA burns easily with heavy dripping that could ignite the cotton on the bottom in a UL-94 test. An illustration of the burning proves is shown in **Scheme 2**. When 2 wt.% of RDP is added to the polymer, the sample could self-extinguish in 2 s, but it also induced heavy dripping due to the fact that RDP is also a liquid plasticizer. When 6 wt.% cellulose was used alone, the dripping was greatly reduced but the sample kept on burning for more than 30 s. Although neither RDP nor cellulose could make the composite pass the V0 criteria, they could significantly improve one of the factors that would lead to V0 grade. Naturally, the idea of combining the two occurred and the addition of only 8 wt.% RDP coated cellulose (CF-RDP) is needed for

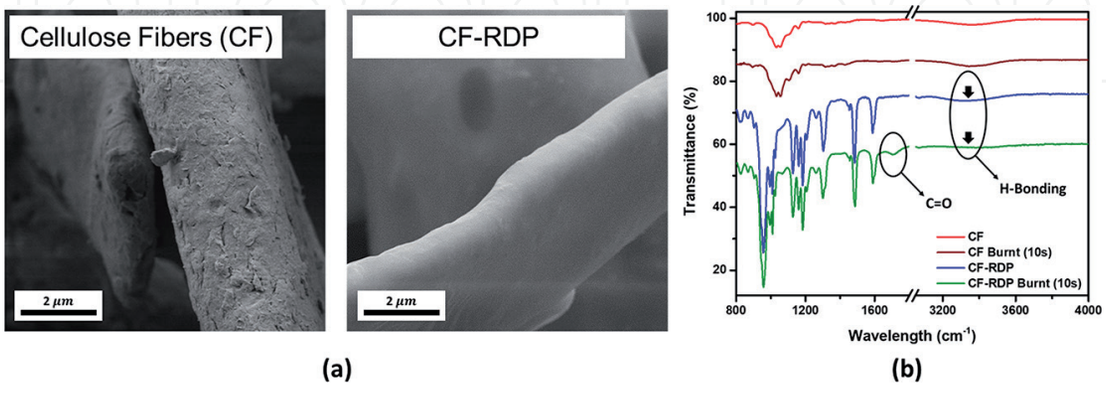

Figure 7. SEM image and FTIR spectra of cellulose fibers: (a) SEM images taken on neat cellulose fiber with and without RDP coating; (b) FTIR spectra of neat cellulose fiber and RDP-cellulose before and after 10s burning. Adapted from Ref. [5]. Copyright (2018) with permission from Elsevier.

the PLA composite to self-extinguish in 2 s and only slight dripping was observed, which is also relatively cold and did not ignite the cotton on the bottom. Further SEM imaging and FTIR tests showed that RDP completely wets the cellulose surface though the hydrogen bond between RDP and cellulose, as shown in **Figure 7**. Cellulose also immobilized RDP which help retained its ability of plasticizing and surface blooming. When PLA/CF-RDP decomposes during combustion, CF-RDP will dehydrate, where it releases water vapor and lower the temperature by absorbing heat. The dehydration of CF-RDP is confirmed by the intensity reduction of the H-bonding on the FTIR spectra.

3. Binary polymer system

Melt blending two different polymers together is one of the simplest way to produce a new material with combined properties. Yet most polymers tend to phase separate due to the large unfavorable enthalpy [38–40]. Although the block or graft copolymers could easily solve the problem, the synthesizing procedure is often system specific and expensive for industrial applications [41]. Thus, research on numerous possible compatibilizers have been done over several decades [42–45]. As briefly mentioned before, Araki et al. have developed a theory for explaining the effect of clay in compatibilizing polymer blends [30]. Two types of polymer blends were studied: polystyrene/poly(methyl methacrylate) (PS/PMMA) blend stands for when only one polymer has a favorable interaction with clay; polycarbonate/poly(styrene-co-acrylonitrile) (PC/SAN) blend stands for when both polymers have similar affinity to clay platelets. In both situations, the organoclays have successfully reduced the domain size and phase separation, and the clay platelets appeared to be adsorbed onto the polymer interface and aligned following the contour of the domain. The compatibilizing effect would generally increase with increasing clay concentration. When the domain size is reduced with better compatibility, more interface area is created to contain the increased clay content. However, the clay platelets would start to bend when the domain size is smaller than the clay radius. This would result in increasing the bending energy, as opposed to reducing the system free energy. Thus, the compatibilizing effect of clay could only work to the extend where the minimum domain size is reached. And the minimum domain size is approximately equal to the linear dimension of the filler.

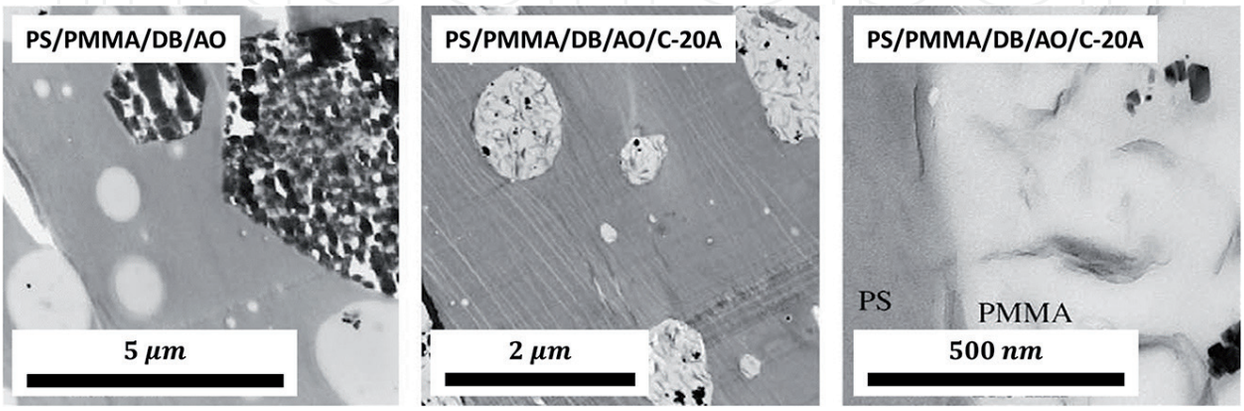

Figure 8. TEM images taken on cross-sections of PS/PMMA composites. Adapted from Ref. [2]. Copyright (2018) with permission from Elsevier.

Based on this theory, Park et al. studied the effect of clay's effect on improving flame retardant efficiency in binary polymer systems [2]. For the PS/PMMA/Microfine AO_3 (AO)/decabromodiphenyl ether (DB) blend, addition of Cloisite 20A clay (C-20A) could significantly improve the dispersion of DB and AO, shown in **Figure 8**, which result in passing the UL-94 V0 grade. C-20A clay was exfoliated in the polymer blend, and the FR agents were attached to the clay surface. Hence, the dispersion of FR agent was also improved and resulted in higher FR efficiency. However, for PC/SAN/DB/AO blend, adding C-20A did not enhance the flame retardant performance. They argue that for this blend, the attraction between clay and FR agent is larger than that between clay and the polymer blend. Thus clay has a lower degree of exfoliation and did not enhance the FR agent's dispersion. Later on, they have also discussed the effect of RDP coating [23]. RDP coated clay was added to both PS/PMMA blend and PC/SAN24 blend and two different morphologies were observed. The RDP coated clay would segregate in the PMMA domain in PS/PMMA blend, whereas it was segregated on the polymer interface in PC/SAC24 blend. This difference is attributed to the interfacial tension difference between RDP with each polymer component, and the interfacial tension of the polymer interface. In PS/PMMA blend, the interfacial tensile of RDP/PS and RDP/PMMA were both larger than that of PS/PMMA interface. In this case, the addition of RDP-clay could not reduce the overall interfacial energy. As a contrast, the interfacial energy of PC/SAN24 interface is higher than that of PC/RDP-clay. Hence, the system interfacial energy would decrease with RDP-clay segregated on the PC/SAN24 interface. Further examination on the flammability of PC/SAN24 blend with RDP-clay also showed that during combustion, the RDP-clay worked against the phase separation and stabilized the polymer blend. RDP helped reducing the brittleness of the protective char layer, which in turn reduced the heat release rate and mass loss rate.

4. Physical properties

4.1. Impact resistance

It was well known that for singular polymer matrix, the particle size and particle/polymer surface interaction have a great influence on the composite's mechanical properties [46]. By comparing between C-Na^+, C-RDP clay and C-30B clay, Guo et al. [22] concludes that the mechanical properties, such as impact strength and tensile strength, will decrease with increasing degree of exfoliation of the clay particles. This is due to the fact that the magnitude of the internal stress, which generated at the tip of the particle and could form micro-cracks, is in direct proportion to the particle aspect ratio. Given that the aspect ratio of exfoliated clay platelets could be several magnitudes larger than that of clay tactoids, it is easier for the micro-cracks to enlarge and propagate under external stress in the exfoliated polymer/clay blend. Moreover, a similar result was also found in binary polymer blends with clay [47]. When C-Na^+, C-RDP clay and C-30B clay were added to a biodegradable PLA/poly(butylene adipate-*co*-butylene terephthalate) (PBAT) blend, C-30B performs best in reducing the domain size and increasing compatibility between two polymers, as can be seen in **Figure 9**. However, the PLA/PBAT blend with clays showed a rapid and huge reduction on the impact strength even with low clay concentration, as seen in **Figure 10**. This phenomenon is explained by the theory that the clay platelets formed a strong barrier at the polymer interface, which blocked inter-diffusion between two polymers, and as a consequence, the two polymer phases were easily separated under stress.

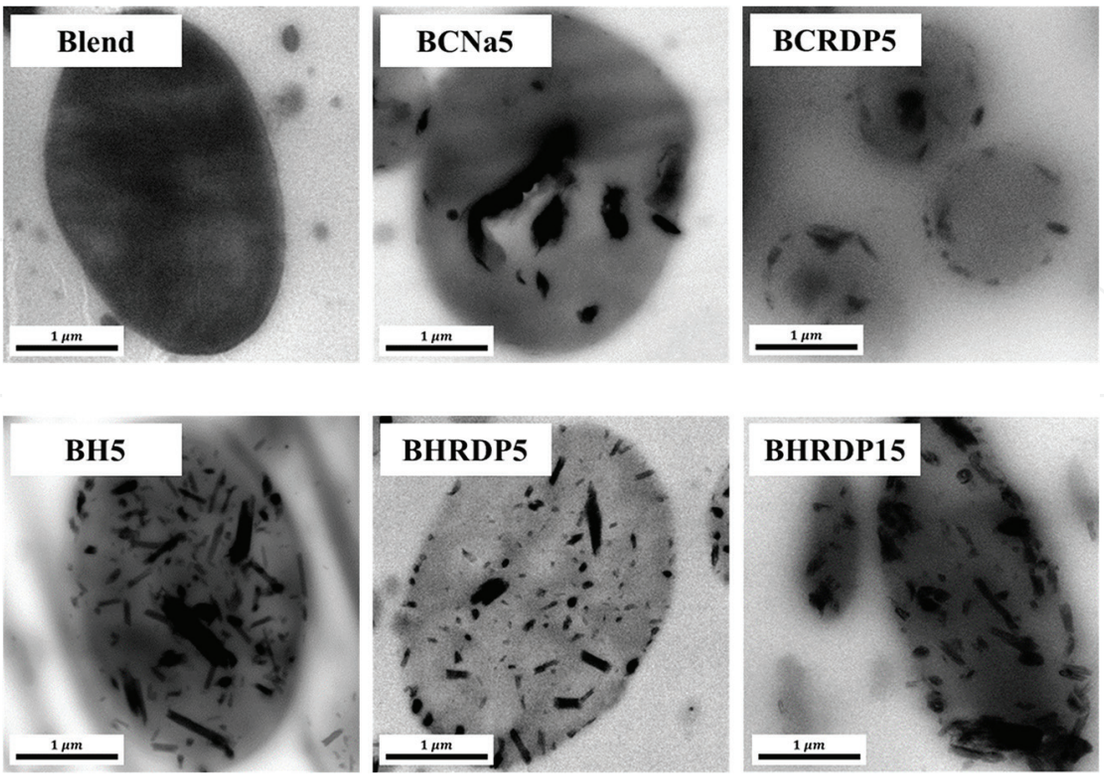

Figure 9. TEM images taken on cross-sections of PLA/PBAT based composites: (Blend) PLA/PBAT; (BCNa5) PLA/PBAT/5 wt.% of C-Na[2]; (BCRDP5) PLA/PBAT/5 wt.% of C-RDP; (BH5) PLA/PBAT/5 wt.% of HNTs; (BHRDP5) PLA/PBAT/5 wt.% of H-RDP; (BHRDP15) PLA/PBAT/15 wt.% of H-RDP. Adapted with permission from Ref. [47]. Copyright (2018) American Chemical Society.

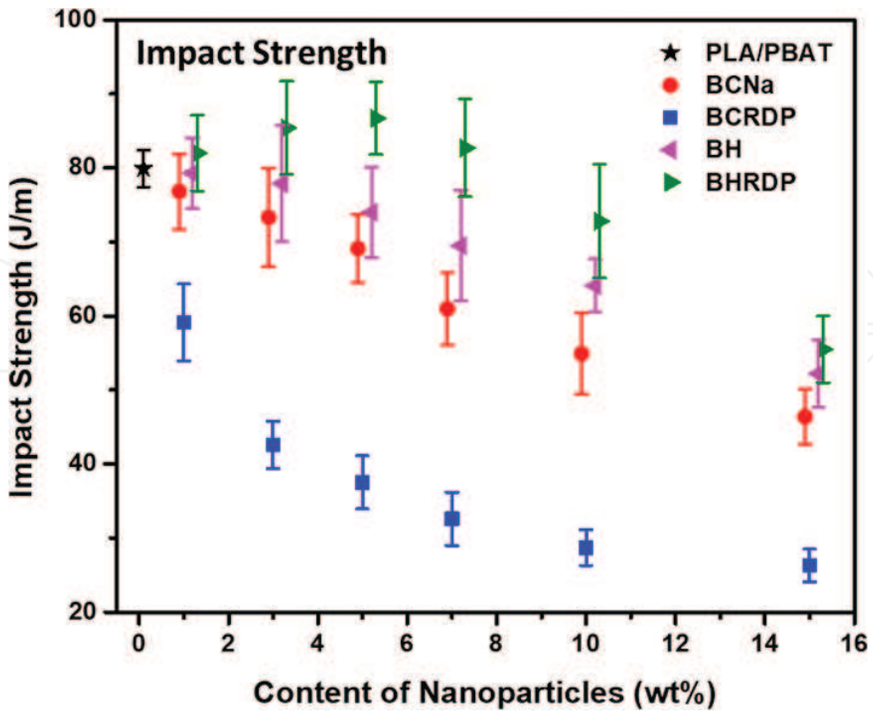

Figure 10. Impact strength of PLA/PBAT based blends. Adapted with permission from Ref. [47]. Copyright (2018) American Chemical Society.

To resolve the problem of the mechanical properties reduction, they discovered that tubular nanoparticles, such as Hollysite nanotubes, would lie perpendicular to the PLA/PBAT polymer interface instead of parallel as the clay, shown in **Figure 9**. Moreover, with this vertical orientation of HNTs particle, a "stitching" effect was observed where the impact strength first increase with the increasing HNTs concentration. The difference of particle orientation between nanotubes and clays is due to the fact that nanotubes are longer and more rigid than clay platelets. Hence, a much larger bending energy is required for nanotubes to lie along the domain curvature. As a result, the system energy is lower when nanotubes lie vertical to the polymer interface. In this way, nanotubes could enhance the interfacial diffusion and reinforce the binary polymer blend.

4.2. Ductility

For polymers that are highly flammable, high loading of flame retardant filler is generally need to render self-extinguish of the composite [48–50], which will significantly reduce the ductility of the material, making the composite hard to process. In the previous discussed three component flame retardant EVA composite [6], EVA/ATH/MoS_2/graphene, the total FR filler loading was reduced from 60 to 40 wt.%, which maintained the elasticity of pure EVA and increased the tensile modulus and tensile strength to equivalent with that of PVC, as summarized in **Table 2**. With careful examination of the individual effect of each component, they discovered that addition of MoS_2 to the EVA/ATH blend decreased the tensile modulus, strength and elongation, while addition of graphene significantly increased these mechanical properties. In the V0 blend containing all three components, the ultimate tensile strength is even higher than the EVA/ATH/graphene blend, which has the highest tensile modulus and elongation at break. This is achieved through the second quasi-elastic response, which is an indication of nanoparticles reinforcing the matrix against scission and polymer chain disentanglement. Thus, the addition of graphene platelets improved the overall FR particle dispersion which provide a larger surface area for polymer chain absorption, while MoS_2 did not have the dispersant effect which lead to reduction of its specific surface area.

Ductility is also an important property which determines the extruding conditions when the polymers are processed. In particular, the recent popularity of FDM printing requires that the ductility of the blends needs to be preserved and allow them to be drawn into uniform

Sample	Young's modulus (MPa)	Tensile strength (MPa)	Elongation at break (%)	Impact toughness (J/cm^3)	UL-94 grade
PVC	6–1120 (avg. 38.8)	1.1–29.0 (avg. 15.6)	80–920 (avg. 308)	N.A.	V-0
EVA/ATH	117.5 ± 8.6	12.6 ± 1.1	359 ± 28	39.3	V-2
EVA/ATH/MoS_2	163.5 ± 9.3	14.1 ± 1.0	306 ± 26	35.0	V-2
EVA/ATH/GNPs	261.6 ± 15.5	19.7 ± 1.6	455 ± 51	72.9	NG
EVA/ATH/MoS_2/GNPs	258.4 ± 12.2	21.5 ± 1.5	448 ± 43	70.7	V-0

Table 2. Tensile properties and impact toughness of EVA based blends. Reproduced from Ref. [6]. Copyright (2018) with permission from Elsevier.

filaments and withstand further drawing through the printer nozzles [51]. As mentioned in previous section [4], the addition of C-30B to PLA/MPP successfully improved the dispersion of MPP which provides a higher flame retardant efficiency. Through comparing the impact strength, the addition of MPP embrittles the PLA composite, while adding C-30B and MPP together restored the impact strength to the same level of pure PLA and even slight higher. Examination of the fracture surface showed that the MPP tactoids would delaminate from the PLA matrix under impact stress. With C-30B localized at the PLA/MMP interface, the micro-cracks brought by MPP tactoids were restricted by the rigid C-30B platelets. Therefore, the impact energy dissipation was improved and the PLA/MPP/C-30B blend was successfully drawn into filaments. The printed PLA/MPP/C-30B sample also achieved V0 grade in the UL-94 test. **Figure 11** summarized the comparison of cone calorimetry test result and mechanical properties between molded and printed PLA/MPP/C-30B sample. The cone calorimetry data of printed sample was similar to the molded one. The impact strength, Young's modulus, tensile strength and elongation of the printed sample was slightly lower than the molded sample, but the difference was within one statistical deviation. This is due to the incomplete fusion between the filaments during printing. Never the less, the printing process does not have a significant influence on the composite performance.

4.3. Gas permeability

Gas permeability is a very important factor for polymer materials used in packaging. Many studies have been established that layered particles have a great effect in enhancing the gas barrier effect [52, 53]. As part of their study on comparing between clay platelets and nanotubes, Guo et al. [22] derived individual equations to calculate the oxygen permeability for blends containing clay or nanotubes:

$$\frac{P}{P_o} = \frac{1-\varnothing}{1+\frac{\alpha}{2}\varnothing} \text{ (for clay)} \tag{1}$$

$$\frac{P}{P_o} = \frac{1-\varnothing}{1+\frac{\pi^2-8}{16}\varnothing} \text{ (for nanotubes)} \tag{2}$$

where, P is gas permeability of polymer with particle, and P_o is gas permeability of polymer without particle. $\varnothing$ is the volume fraction of nanoparticles.α is the aspect ratio of clay platelets. From the equations we could see that the aspect ratio of platelets particle could directly influence the

PLA/MPP/C30B	t_1	t_2	Dripping	Grade	LOI
Molded	1s	2s	N	V0	28.5
Printed	1s	4s	N	V0	28.5

(a)

PLA/MPP/C30B	Impact (J/m)	Modulus (GPa)	Tensile (MPa)	Elongation (%)
Molded	31.1±3.0	4.05±0.14	80.4±4.1	2.61±0.18
Printed	27.4±2.8	3.91±0.22	70.0±3.8	2.32±0.21

(b)

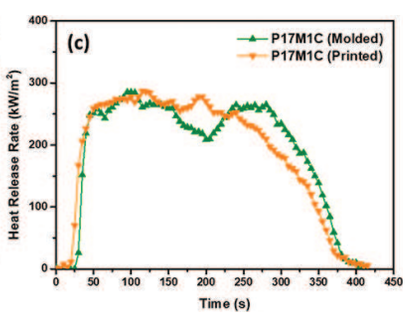

Figure 11. Comparison between molded and 3D printed PLA/MPP/C-30B blend: (a) UL-94 test results; (b) mechanical properties; (c) cone calorimetry test result. Adapted from Ref. [4]. Copyright (2018) with permission from Elsevier.

http://dx.doi.org/10.5772/intechopen.79548

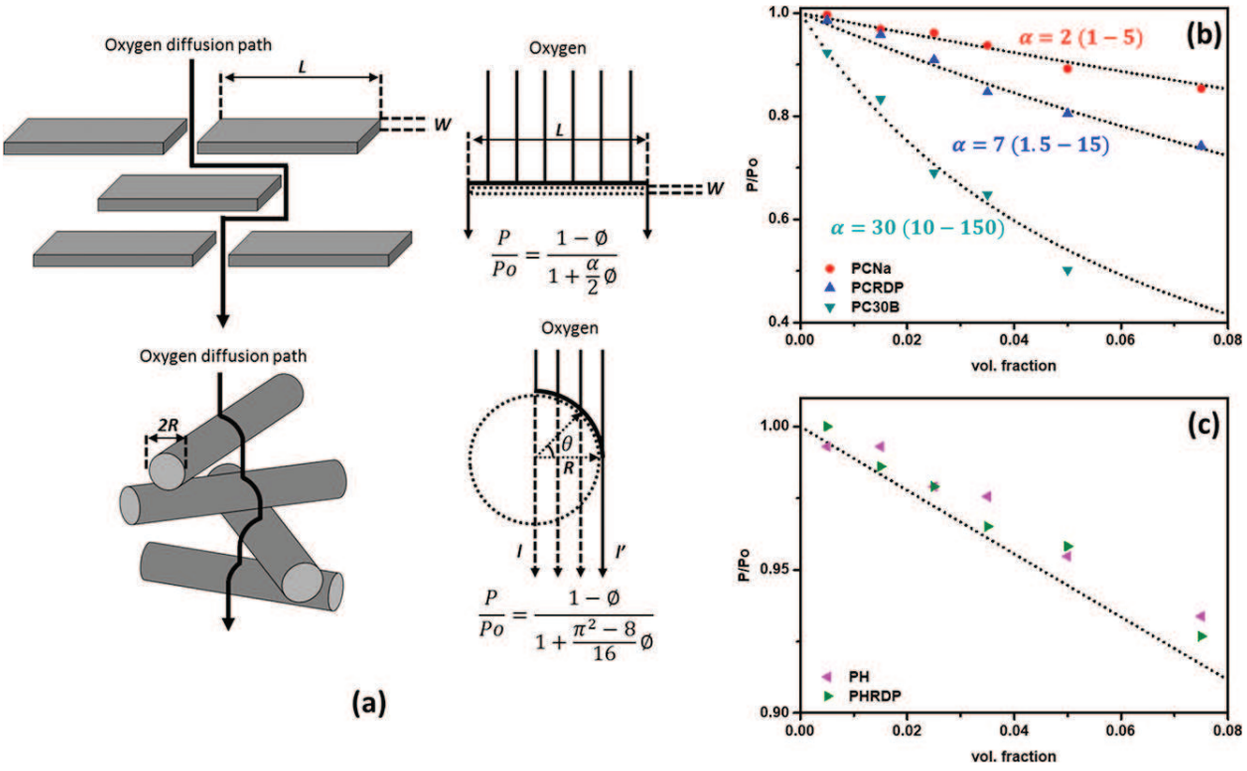

Figure 12. Gas permeability results of PLA based blends: (a) an illustration of oxygen pathway in PLA blends with clay or nanotubes; (b) comparison between calculated (dotted line) and measured values of gas permeability of PLA/clay blends; (c) comparison between calculated (dotted line) and measured values of gas permeability of PLA/nanotubes blends. Adapted from Ref. [22]. Copyright (2018) with permission from Elsevier.

gas permeability, whereas for tubular particles the gas permeability is independent on its dimension. **Figure 12** shows the comparison between the measured gas permeability and the calculated value, and a scheme of the possible pathway in PLA blends with clay or nanotubes. For clay particles, when calculating the gas permeability with the dimension of single clay platelets, the calculated result is higher than the measured result. By back calculating the α value from the measured gas permeability, the values are equivalent to the aspect ratio of the tactoids, instead of dimension of the clay platelets. Therefore, the gas permeability of polymer/clay blend is directly affected by the work of adhesion (W_a) between the polymer and the clay surface. When W_a increases, the clay platelets have a higher degree of exfoliation in the polymer matrix, which result in a smaller tactoid aspect ratio and produces low gas permeability result. On the other hand, the measured gas permeability data for polymer/HNTs blend and polymer/H-RDP blend showed only slight decreasing with increasing nanotubes concentration. This result is in good agreement with the previous equation. Moreover, there is not much difference between the gas permeability data of polymer/HNTs and polymer/H-RDP, which is in agreement with the slight difference on their W_a. In conclusion, clay platelets have a higher barrier effect than nanotubes due to their structure difference, and the barrier effect will increase with increasing degree of exfoliation.

4.4. Thermal conductivity

In addition to its compatibilizing effect and char promotion effect, the high thermal conductivity of graphene has drawn a great attention as well. Kai et al. melt blended graphene with polypropylene (PP) [54]. PP blends with carbon black and Cu microparticles, which also have

Sample	Particle concentration (wt.%)	Thermal conductivity (W/mK)
PP	100/0	0.23
PP/Cu	80/20	0.29
PP/carbon black	80/20	0.36
PP/GNPs	80/20	0.57
	70/30	1.12
	60/40	2.02
	50/50	2.31

Table 3. Thermal conductivity of PP based composites. Reproduced from Ref. [55] with open access.

high thermal conductivity, were also prepared. They found that at the same filler loading, the thermal conductivity of PP/graphene blend is two times higher than that of pure PP, as seen in **Table 3**, whereas the addition of carbon black or Cu only slightly increased the thermal conductivity. This effect is contributed to the large aspect ratio of graphene. The large surface area of graphene provides a better coupling between polymer chains and graphene. Comparing to the spherical structure of carbon black and Cu, it is easier for graphene platelets to form an efficient heat transfer path inside the polymer matrix. They also measured the thermal conductivity of PP/graphene at different graphene loading, and found that the thermal conductivity increased linearly with graphene concentration up to 50% graphene loading. Zhang et al. have stated that up to approximately 30 vol.% of filler, the thermal conductivity will first increase linearly with filler loading due to the increase in the contact area between filler and the polymer matrix [55]. Then the slop of this linear relationship will decrease because the filler starts to agglomerate within the polymer matrix and the conductive pathway was destructed. Thus, the linear relationship found by Kai et al. indicated that graphene platelets were uniformly distributed in the PP matrix. At 40% graphene loading, the thermal conductivity of PP/graphene blend is 2.0 W/mK, which is the same with flue gas in a metal heat exchanger. This result opens up the possibility of PP/graphene blends used in the application of heat exchanger which is also corrosion resistance and easy to process.

4.5. Rheology

In general, since the addition of fillers will restrict polymer chain movement, they will reinforce the polymer matrix in the rheological response. The efficiency of the reinforcement is related to the interaction between the filler and the polymer matrix. Through the comparison between the G′ dependency on frequency of PLA blend with C-Na^+, C-RDP and C-30B, Guo et al. [22] discovered that PLA/C-30B has the lowest slop at low frequency, and it is related to the fact that C-30B has the highest degree of exfoliation comparing to C-Na^+ and C-RDP, shown in **Figure 13**. PLA blends with HNTs and H-RDP have the similar result to PLA/C-30B, which indicates the nanotubes are very effective in restrict the polymer chain motion. Moreover, the PLA/H-RDP blend have a better performance than PLA/HNTs blend, which is due to the higher affinity (W_a) between the PLA and particles induced by RDP coating. When

http://dx.doi.org/10.5772/intechopen.79548

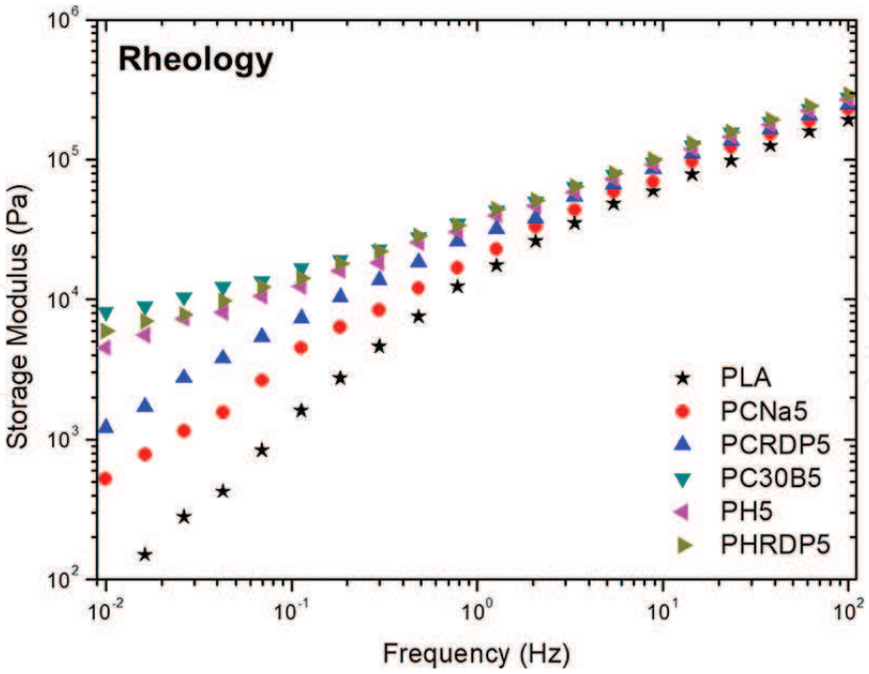

Figure 13. Rheology performance of PLA based composites. Adapted from Ref. [22]. Copyright (2018) with permission from Elsevier.

utilized in flame retardant composites, using RDP alone will decrease the G′, which results in swelling the polymer chain and reducing the strength, and also caused heavily dripping during UL-94 test [5]. By adding cellulose to the PLA matrix, the G′ was increased at low frequency, which resulted in prevent deformation and reduce dripping during combustion. Replacing cellulose by RDP coated cellulose, the G′ further increased slightly showing that the RDP coating would increase the interaction between the polymer and the cellulose fiber. Hence, the RDP coated cellulose has a higher efficiency in prevent deformation upon heating and prevent dripping during combustion.

For binary polymer systems, the morphology of the polymer phase separation and filler location play a significant role in the rheological response. In previous section, Guo, et al. [47, 56] showed that the addition of C-30B and C-RDP could effectively increase the compatibility between PLA and PBAT, while reducing the impact strength due to the strong barrier effect at the polymer interface. HNTs and H-RDP were not as effective at reducing the domain size and increasing the polymer compatibility, but the impact strength was enhanced with the "stitching" effect of nanotubes. The rheological response of PLA/PBAT blends were plotted in **Figure 14**, they found that the G′ of PLA/PBAT/C-30B and PLA/PBAT/C-RDP were both three magnitudes higher than PLA/PBAT control blend. This is attributed to the strong interaction between clay platelets and the polymers. However, at higher strain amplitude, both PLA/PBAT/C-30B and PLA/PBAT/C-RDP sample showed a G′ peak. This is identified as a stick slip motion caused by polymer chain confinement due to clay platelets blocking the polymer chain entanglement. On the G′ curve of PLA/PBAT/H-RDP blend, no peak was observed. This is also attributed to the nanotubes stay perpendicular to the polymer interface, and therefore the entanglement between two polymers was not affected.

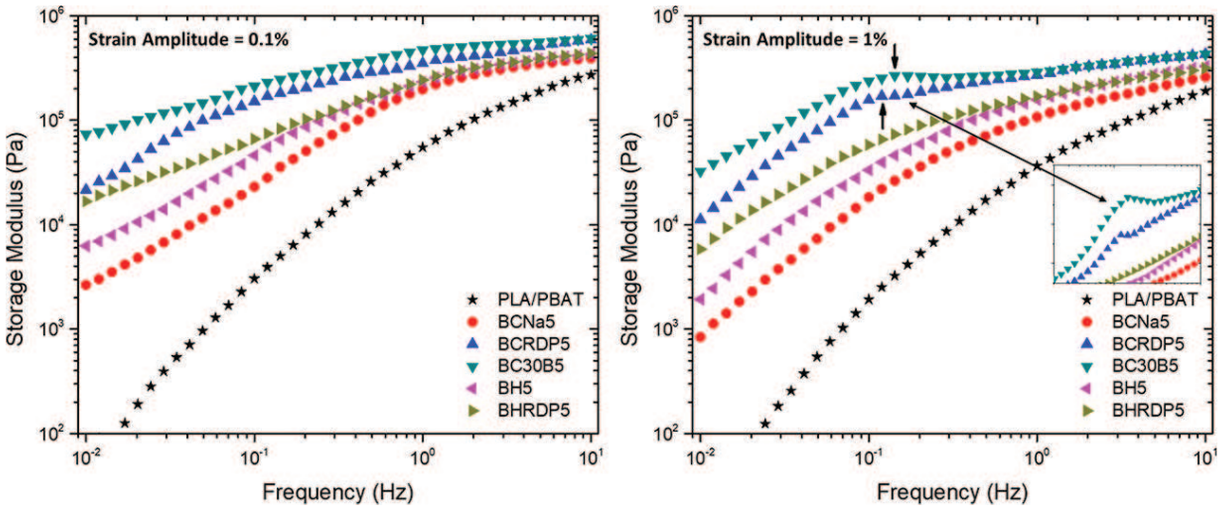

Figure 14. Rheology response of PLA/PBAT blends with clays or nanotubes. Adapted with permission from Ref. [47]. Copyright (2018) American Chemical Society.

5. Conclusion

We first reviewed the interaction between three widely used nanoparticles and singular polymer matrix. As being reported, the affinity between the nanoparticle and polymer could be determined by measuring the Young's contact angle and calculating the work of adhesion (W_a). With a higher W_a, the nanoparticle will generally achieve a higher degree of exfoliation inside the polymer matrix. In a polymer composite where flame retardant particles tend to form agglomerates, the high exfoliated nanoparticle could act as a dispersant. They will segregate at the polymer/FR particle interface and increase the interaction between these two. As a result, the dispersion of the flame retardant particle is improved, as well as a higher flame retardant efficiency, which will render the polymer composite pass the V0 rating in UL-94 test at a lower filler content. We also looked at the surface interaction of nanoparticles in binary polymer systems, they perform in a similar mechanism as in the singular polymer system, where the dispersion of the flame retardant additive is improved and the phase separation is reduced. Moreover, the addition of the nanoparticles has a significant influence on the mechanical properties of the polymer composite. In a singular polymer matrix, when clay platelets were added, the impact strength will decrease with increasing degree of clay exfoliation, due to the high magnitude of internal stress created at the tip of exfoliated clay platelets. In binary polymer blends, the addition of clay will also decrease the impact resistance by localizing at the polymer interface and blocking the polymer chain entanglement across the interface. Tubular nanoparticle, on the other hand, will lie perpendicular to the polymer interface, which will enhance the impact and tensile properties by a "stitching" effect. Rheology performance was affected in the similar way as the impact and tensile properties. Clay has also been proved to have a higher improvement on the gas barrier effect than tubular particles. Large aspect ratio particles with high thermal conductivity, such as graphene, could also be used in applications for developing corrosion-resistant polymer composites for heat exchangers. In sum, the usage of nanoparticles could greatly increase the flame retardant efficiency by improving the filler dispersion in the polymer matrix, as well as other physical properties.

Author details

Yuan Xue, Yichen Guo* and Miriam H. Rafailovich

*Address all correspondence to: guoichen@gmail.com

Department of Materials Science and Engineering, Stony Brook University, New York, USA

References

[1] Lubin G. Handbook of Composites. Springer Science & Business Media; 2013

[2] Pack S et al. Mode-of-action of self-extinguishing polymer blends containing organoclays. Polymer Degradation and Stability. 2009;**94**(3):306-326

[3] Si M et al. Self-extinguishing polymer/organoclay nanocomposites. Polymer Degradation and Stability. 2007;**92**(1):86-93

[4] Guo Y et al. Engineering flame retardant biodegradable polymer nanocomposites and their application in 3D printing. Polymer Degradation and Stability. 2017;**137**:205-215

[5] Guo Y et al. Incorporation of cellulose with adsorbed phosphates into poly (lactic acid) for enhanced mechanical and flame retardant properties. Polymer Degradation and Stability. 2017;**144**:24-32

[6] Guo Y et al. Capitalizing on the molybdenum disulfide/graphene synergy to produce mechanical enhanced flame retardant ethylene-vinyl acetate composites with low aluminum hydroxide loading. Polymer Degradation and Stability. 2017;**144**:155-166

[7] Li N et al. Influence of antimony oxide on flammability of polypropylene/intumescent flame retardant system. Polymer Degradation and Stability. 2012;**97**(9):1737-1744

[8] Alaee M et al. An overview of commercially used brominated flame retardants, their applications, their use patterns in different countries/regions and possible modes of release. Environment International. 2003;**29**(6):683-689

[9] Sain M et al. Flame retardant and mechanical properties of natural fibre–PP composites containing magnesium hydroxide. Polymer Degradation and Stability. 2004;**83**(2):363-367

[10] Wang D-Y et al. Preparation and burning behaviors of flame retarding biodegradable poly (lactic acid) nanocomposite based on zinc aluminum layered double hydroxide. Polymer Degradation and Stability. 2010;**95**(12):2474-2480

[11] Zhang S et al. Intercalation of phosphotungstic acid into layered double hydroxides by reconstruction method and its application in intumescent flame retardant poly (lactic acid) composites. Polymer Degradation and Stability. 2018;**147**:142-150

[12] Wang X et al. Controllable fabrication of zinc borate hierarchical nanostructure on brucite surface for enhanced mechanical properties and flame retardant behaviors. ACS Applied Materials & Interfaces. 2014;**6**(10):7223-7235

[13] Chen S et al. Intumescent flame-retardant and self-healing superhydrophobic coatings on cotton fabric. ACS Nano. 2015;**9**(4):4070-4076

[14] Zhu C et al. Synthesis and application of a mono-component intumescent flame retardant for polypropylene. Polymer Degradation and Stability. 2018;**151**:144-151

[15] Baekeland LH. Bakelite, a new composition of matter: Its synthesis, constitution, and uses. Scientific American, Suppl. 1909;**68**:322

[16] Goodyear C. Dinglers Polytechnisches Journal. 1856;**139**:376

[17] Balazs AC, Emrick T, Russell TP. Nanoparticle polymer composites: Where two small worlds meet. Science. 2006;**314**(5802):1107-1110

[18] Morgan AB, Wilkie CA. Practical Issues and Future Trends in Polymer Nanocomposite Flammability Research. New York, NY, USA: John Wiley & Sons; 2007

[19] Laoutid F et al. New prospects in flame retardant polymer materials: from fundamentals to nanocomposites. Materials Science and Engineering: R: Reports. 2009;**63**(3):100-125

[20] Ray SS et al. New polylactide/layered silicate nanocomposite: Nanoscale control over multiple properties. Macromolecular Rapid Communications. 2002;**23**(16):943-947

[21] <MSDS - Quaternary Ammonium Chloride.pdf>.

[22] Guo Y et al. Effects of clay platelets and natural nanotubes on mechanical properties and gas permeability of poly(lactic acid) nanocomposites. Polymer. 2016;**83**:246-259

[23] Pack S et al. Role of surface interactions in the synergizing polymer/clay flame retardant properties. Macromolecules. 2010;**43**(12):5338-5351

[24] Modro AM, Modro TA. The phosphoryl and the carbonyl group as hydrogen bond acceptors. Canadian Journal of Chemistry. 1999;**77**(5-6):890-894

[25] Jang BN, Wilkie CA. The effects of triphenylphosphate and recorcinolbis(diphenylp hosphate) on the thermal degradation of polycarbonate in air. Thermochimica Acta. 2005;**433**(1):1-12

[26] Granzow A. Flame retardation by phosphorus compounds. Accounts of Chemical Research. 1978;**11**(5):177-183

[27] Gross RA, Kalra B. Biodegradable polymers for the environment. Science. 2002;**297**(5582): 803-807

[28] Bourbigot S, Fontaine G. Flame retardancy of polylactide: An overview. Polymer Chemistry. 2010;**1**(9):1413-1422

[29] Fontaine G, Bourbigot S. Intumescent polylactide: A nonflammable material. Journal of Applied Polymer Science. 2009;**113**(6):3860-3865

[30] Si M et al. Compatibilizing bulk polymer blends by using organoclays. Macromolecules. 2006;**39**(14):4793-4801

[31] Lee C et al. Measurement of the elastic properties and intrinsic strength of monolayer graphene. Science. 2008;**321**(5887):385-388

[32] Stankovich S et al. Graphene-based composite materials. Nature. 2006;**442**(7100):282

[33] Feng X et al. Studies on synthesis of electrochemically exfoliated functionalized graphene and polylactic acid/ferric phytate functionalized graphene nanocomposites as new fire hazard suppression materials. ACS Applied Materials & Interfaces. 2016;**8**(38):25552-25562

[34] Sinha Ray S et al. New polylactide/layered silicate nanocomposites. 1. Preparation, characterization, and properties. Macromolecules. 2002;**35**(8):3104-3110

[35] Jonoobi M et al. Mechanical properties of cellulose nanofiber (CNF) reinforced polylactic acid (PLA) prepared by twin screw extrusion. Composites Science and Technology. 2010;**70**(12):1742-1747

[36] Iwatake A, Nogi M, Yano H. Cellulose nanofiber-reinforced polylactic acid. Composites Science and Technology. 2008;**68**(9):2103-2106

[37] Lu Y et al. Improved mechanical properties of polylactide nanocomposites-reinforced with cellulose nanofibrils through interfacial engineering via amine-functionalization. Carbohydrate Polymers. 2015;**131**:208-217

[38] Bates FS. Polymer-polymer phase behavior. Science. 1991;**251**(4996):898-905

[39] Van de Witte P et al. Phase separation processes in polymer solutions in relation to membrane formation. Journal of Membrane Science. 1996;**117**(1-2):1-31

[40] Nishi T, Wang T, Kwei T. Thermally induced phase separation behavior of compatible polymer mixtures. Macromolecules. 1975;**8**(2):227-234

[41] Paul DR, Bucknall CB. Polymer Blends. Wiley; 2000

[42] Tanaka H, Lovinger AJ, Davis DD. Pattern evolution caused by dynamic coupling between wetting and phase separation in binary liquid mixture containing glass particles. Physical Review Letters. 1994;**72**(16):2581

[43] Ginzburg VV et al. Simulation of hard particles in a phase-separating binary mixture. Physical Review Letters. 1999;**82**(20):4026

[44] Zhou Y et al. Nanorods with different surface properties in directing the compatibilization behavior and the morphological transition of immiscible polymer blends in both shear and shear-free conditions. Macromolecules. 2018;**51**(8):3135-3148

[45] Cho KY et al. Highly enhanced electromechanical properties of PVDF-TrFE/SWCNT nanocomposites using an efficient polymer compatibilizer. Composites Science and Technology. 2018;**157**:21-29

[46] Fu S-Y et al. Effects of particle size, particle/matrix interface adhesion and particle loading on mechanical properties of particulate–polymer composites. Composites Part B: Engineering. 2008;**39**(6):933-961

[47] Guo Y et al. Enhancing the mechanical properties of biodegradable polymer blends using tubular nanoparticle stitching of the interfaces. ACS Applied Materials & Interfaces. 2016;**8**(27):17565-17573

[48] Hoffendahl C et al. The combination of aluminum trihydroxide (ATH) and melamine borate (MB) as fire retardant additives for elastomeric ethylene vinyl acetate (EVA). Polymer Degradation and Stability. 2015;**115**:77-88

[49] Yen Y-Y, Wang H-T, Guo W-J. Synergistic flame retardant effect of metal hydroxide and nanoclay in EVA composites. Polymer Degradation and Stability. 2012;**97**(6):863-869

[50] Cavodeau F et al. Fire retardancy of ethylene-vinyl acetate composites—Evaluation of synergistic effects between ATH and diatomite fillers. Polymer Degradation and Stability. 2016;**129**:246-259

[51] Krishnaswamy RK. Analysis of ductile and brittle failures from creep rupture testing of high-density polyethylene (HDPE) pipes. Polymer. 2005;**46**(25):11664-11672

[52] Sinha Ray S et al. Polylactide-layered silicate nanocomposite: A novel biodegradable material. Nano Letters. 2002;**2**(10):1093-1096

[53] Tenn N et al. Effect of nanoclay hydration on barrier properties of PLA/montmorillonite based nanocomposites. The Journal of Physical Chemistry C. 2013;**117**(23):12117-12135

[54] Yang K et al. The thermo-mechanical response of PP nanocomposites at high graphene loading. Nano. 2015;**1**(3):126-137

[55] Zhang S et al. The effects of particle size and content on the thermal conductivity and mechanical properties of Al_2O_3/high density polyethylene (HDPE) composites. Express Polymer Letters. 2011;**5**(7):581-590

[56] Guo Y et al. Enhancing impact resistance of polymer blends via self-assembled nanoscale interfacial structures. Macromolecules. 2018;**51**(11):3897-3910